ACS OMEGA

Open Access

http://pubs.acs.org/journal/acsodf

Article

Study on the Drying Kinetics of Zinc Smelting Iron Slag Assisted by Ultrasonic Waves

Yue Cheng, Linqing Dai,* Libo Zhang, Bo Yu, Chuxuan Yang, Liang Zhou, and Baichuan Lou

Cite This: *ACS Omega* 2024, 9, 2578−2584

Read Online

ACCESS | Metrics & More | Article Recommendations

ABSTRACT: This study investigates the impact of ultrasonic treatment on the drying kinetics of zinc smelting iron slag. Through the Arrhenius equation, it was found that the reaction order of zinc smelting iron slag remains constant at 1/2 before and after ultrasonic treatment, indicating a proportional relationship between the reaction rate and the square root of the reactant concentration. Despite the increased drying rate of the iron slag due to ultrasonic pretreatment, the reaction order remains at 1/2. Additionally, it was observed that the drying kinetics of untreated iron slag aligns with the Wang and Singh model, while the drying kinetics of ultrasonically pretreated iron slag fits the Page model. The Page model facilitates the prediction of drying rate and drying time for ultrasonically pretreated iron slag, enabling the optimization of the drying process, enhancing efficiency, and comparing drying performance under different conditions. Using ultrasonic pretreatment, the subsequent drying process of iron slag can significantly shorten the time and save energy. These findings provide essential theoretical foundations for optimizing the drying process of zinc smelting iron slag.

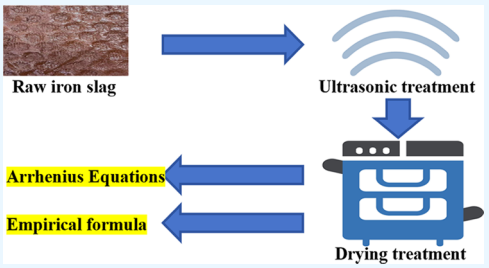

1. INTRODUCTION

Zinc resources are nonrenewable and are becoming increasingly scarce with continuous exploitation and use.[1−3] Consequently, low-grade zinc ores and zinc-containing wastes are receiving increased attention, with researchers exploring ways to extract valuable metals from them.[4,5] Iron slag, a solid waste produced during the purification and impurity removal stage of the wet zinc smelting process, is of particular interest. Wet zinc smelting, which accounts for over 85% of the world's zinc production, has become the dominant method for zinc smelting.[6−8] Iron slag, with its high iron and zinc content, has significant potential for comprehensive recovery and utilization.[9,10] However, as a viscous material, iron slag retains a high moisture content of over 40% even after treatment with a plate and frame filter press.[11−13] This high moisture content can cause slag dampness and stickiness, leading to clumping that severely affects the feeding systems of rotary kilns and smelting furnaces.[14,15] This can result in furnace feed disruptions, large fluctuations in furnace conditions, a decrease in zinc oxide quality, and increased labor intensity for workers.[16,17] Moreover, the high moisture content of iron slag makes subsequent dehydration processes difficult and energy-intensive.[18,19]

Some companies currently use dehydration agents to pretreat iron slag.[20,21] However, this approach has drawbacks including long conditioning times, high costs, and the introduction of impurities. Ultrasonics is a new water treatment technology that, compared to traditional water treatment technologies, has fewer stringent requirements, shorter action times, and simpler operations. By applying ultrasonic treatment to iron slag before it enters the plate and frame filter press, the existing mature process flow is not altered. Ultrasonics has already been widely used to improve sludge dewatering performance and promote drying in coal and food industries.[22−24]

To date, no one has studied the impact of ultrasound on the drying performance of iron slag. The aim of this study is to use the Arrhenius equation to investigate whether chemical changes occur in the drying process of iron slag before and after ultrasonic treatment. Furthermore, the study aims to derive a suitable semiempirical mathematical kinetic model to describe the isothermal drying characteristics of iron slag after ultrasonic pretreatment.

2. MATERIALS AND METHODS

2.1. Raw Material Analysis. The iron slag used in the experiment was sourced from a zinc smelting company in Yunnan. Its chemical composition is presented in Table 1. From the table, it is evident that the iron slag has the highest zinc (Zn) content, followed by iron (Fe), and it also contains significant amounts of sulfur (S), calcium (Ca), and arsenic (As). The iron slag samples were placed in a constant-temperature drying oven set at 105 °C until a constant weight

Received: September 23, 2023
Revised: November 29, 2023
Accepted: December 20, 2023
Published: January 4, 2024

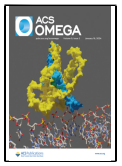

https://doi.org/10.1021/acsomega.3c07344
ACS Omega 2024, 9, 2578−2584

Table 1. Main Chemical Composition of Iron Slag

element	Zn	Fe	S	Ca	As	Al	Pd
%	19.73	15.37	9.79	6.34	1.60	0.9	1.13
element	Si	Mn	Cd	F	Cl	Cu	others
%	0.5	0.02	0.17	0.064	0.018	0.06	44.308

was achieved. The experiment was repeated five times, and the highest and lowest values were excluded. The remaining three results were averaged, revealing a moisture content of 40.1% for the iron slag.

2.2. Experimental Methods. Iron slag samples were divided into two groups, with 15 g taken from each, prepared according to a liquid-to-solid ratio of 4:1, and placed in beakers. One group underwent pretreatment under an ultrasonic frequency of 20 kHz, an ultrasonic power of 70 W, and an ultrasonic duration of 20 s, while the other group was left untreated. Both groups of iron slag were then filtered under the same pressure. Filter cakes of the same weight were placed in an oven and dried at 105 °C. The weight was measured every 5 min until the weight change was less than 0.1 g, marking the end of the drying process.

2.3. Experimental Formula. *2.3.1. Arrhenius Equation.* To study the drying kinetics of iron slag in zinc smelting, we can consider the isothermal drying process of the slag as the thermal evaporation of moist slag, resulting in dried slag and water as products. In order to analyze the drying weight loss curve of the slag, we can employ the isothermal thermogravimetric analysis (TGA) method. In the field of isothermal and heterogeneous reaction kinetics, the widely used reaction kinetics equation is the Arrhenius equation,[25−27] proposed by the Swedish chemist Arrhenius based on thermodynamic principles

$$K = A\ e^{-E/RT} \tag{1}$$

A = frequency factor or pre-exponential factor, s^{-1}; E = activation energy, kJ/mol; R = universal gas constant, R = 8.314 J/(mol·K); and T = absolute temperature, K.

The Arrhenius equation has been extensively validated by experimental data, and the thermal drying process of iron slag can be expressed in the following form

$$d\alpha/dt = A\ e^{-E/RT} f(\alpha) = A\ e^{-E/RT}(1-\alpha)^n \tag{2}$$

α = solid content of iron slag, n = reaction order, and t = drying time.

The solid content α of iron slag can be defined as the percentage of the mass of moisture lost from the iron slag at a certain drying time relative to the total mass of moisture loss. This can be expressed as

$$\alpha = \frac{W_0 - W}{W_0 - W_\infty} = \frac{\Delta W}{\Delta W_\infty} \tag{3}$$

W_0 = initial mass, W = mass at a certain drying time, W_∞ = final mass, ΔW = weight loss at a certain time, and ΔW_∞ = maximum weight loss.

Through the investigation of the kinetics of iron slag, the kinetic factors of the reaction described by eq 2 can be determined, namely, the activation energy E, pre-exponential factor A, and the reaction order n in the reaction mechanism function $f(\alpha) = (1-\alpha)^n$.

To determine the reaction order n in the reaction mechanism function $f(\alpha) = (1-\alpha)^n$, an integral form of the kinetic mechanism function $G(\alpha)$ is introduced. The relationship between the integral form and the differential form of the mechanism function can be seen in eq 4

$$G(\alpha) = \int_0^t A\ e^{-E/RT}\ dt = kt \tag{4}$$

Table 2 shows the results of using eq 2 to calculate the integral form mechanism function $G(\alpha)$ for different reaction orders, based on their differential form mechanism function $f(\alpha)$.

Table 2. Commonly Used Kinetic Reaction Mechanism Functions

number of reaction progressions (n)	differential form $f(\alpha)$	points form $G(\alpha)$
0	1	α
1/2	$(1-\alpha)^{1/2}$	$2 \times [1-(1-\alpha)^{1/2}]$
2/3	$(1-\alpha)^{1/3}$	$3 \times [1-(1-\alpha)^{1/3}]$
1	$(1-\alpha)$	$-\ln(1-\alpha)$
2	$(1-\alpha)^2$	$(1-\alpha)^{-1} - 1$

2.3.2. Empirical Formula. The moisture ratio (MR) versus the time curve in iron slag can reflect the speed of the drying process. The formula for MR is as follows

$$MR = \frac{X_t - X_e}{X_0 - X_e} \tag{5}$$

X_t = the dry basis moisture content of the iron slag at time t (g/g), X_e = the dry basis moisture content of the iron slag at equilibrium (g/g), and X_0 = the initial moisture content of the iron slag (g/g).

Due to the relatively small dry basis moisture content X_e of the iron slag at equilibrium, it is neglected and considered as zero in this study. Therefore, eq 5 is simplified as follows

$$MR = \frac{X_t}{X_0} \tag{6}$$

The dry basis moisture content X of the iron slag is defined as the ratio of the mass of moisture in the iron slag to the mass of bone-dry iron slag. The formula is as follows

$$X = \frac{M}{M_0} \tag{7}$$

M = the mass of pure water in the iron slag (g) and M_0 = the mass of bone-dry iron slag (g).

According to numerous studies conducted by scholars both domestically and internationally on the drying models of wet porous materials, this paper has selected five representative semiempirical and empirical formulas to describe the drying kinetics model of iron slag.[28,29] These formulas are presented in Table 3.

The degree of fit between the predicted values and experimental values of a mathematical model can be evaluated using the following metrics: the correlation coefficient (R^2), chi-square (χ^2), root-mean-square error (RMSE), and sum of squares error (SSE). These formulas are as follows

$$R^2 = \frac{\sum_{i=1}^{n}(MR_i - MR_{pre,i}) \times \sum_{i=1}^{n}(MR_i - MR_{exp,i})}{\sqrt{[\sum_{i=1}^{n}(MR_i - MR_{pre,i})^2]} \times [\sum_{i=1}^{n}(MR_i - MR_{exp,i})^2]} \tag{8}$$

https://doi.org/10.1021/acsomega.3c07344
ACS Omega 2024, 9, 2578−2584

Table 3. Iron Slag Drying Empirical Model

index number	model name	model equations	linear expression
1	Henderson and Pbis	$M_r = \exp(-kt)$	$-\ln \mathrm{MR} = rt$
2	Wang and Singh	$\mathrm{MR} = 1 + at + bt^2$	$\mathrm{MR} = 1 + at + bt^2$
3	Page	$\mathrm{MR} = \exp(-kt^n)$	$\ln(-\ln \mathrm{MR}) = \ln k + n \ln t$
4	Lewis	$\mathrm{MR} = \exp(-kt)$	$\ln \mathrm{MR} = -kt$
5	Wang	$\mathrm{MR} = a \exp(-kt^n)$	$\ln \mathrm{MR} = -kt^n + \ln a$

$$X^2 = \frac{\sum_{i=1}^{n} (\mathrm{MR}_i - \mathrm{MR}_{\mathrm{pre},i})^2}{N - n} \quad (9)$$

$$\mathrm{SSE} = \sum_{i=1}^{N} (\mathrm{MR}_{\mathrm{pre},i} - \mathrm{MR}_{\mathrm{exp},i})^2 \quad (10)$$

$\mathrm{MR}_{\mathrm{exp},i}$ = the moisture content of the ith sample in the drying experiment, $\mathrm{MR}_{\mathrm{pre},i}$ = the predicted moisture content of the ith sample using the model, N = the number of data points measured in the experiment, and n = the number of model parameters.

3. EXPERIMENTAL RESULTS AND DISCUSSION

3.1. Arrhenius Equation Test for Raw Iron Slag. The iron slag samples were subjected to drying at a temperature of 105 °C, and the resulting drying curve of the iron slag was used for kinetic model calculations. The variation of the solid content in the iron slag under the previously mentioned operational conditions is shown in Figure 1.

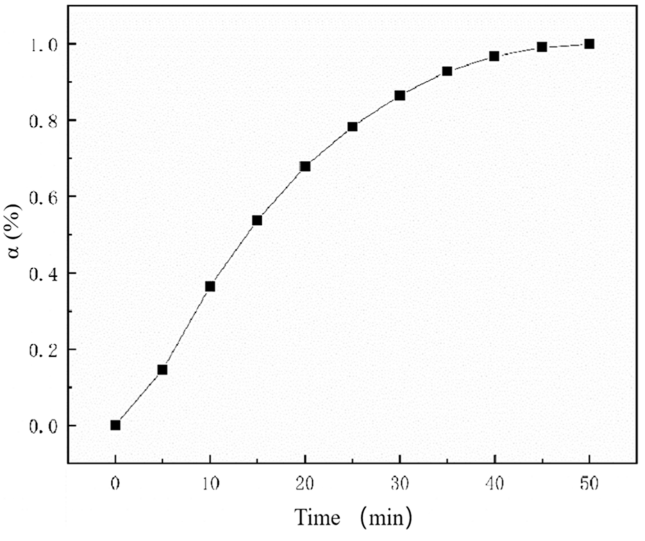

Figure 1. Characteristics of solid content variation of raw iron slag.

The relationship between the solid content of untreated iron slag and drying time, as obtained from the experimental data in Figure 1, was used to determine the integral form of the kinetic model function $G(\alpha)$ for different values of n (n = 0, 1/2, 2/3, and 1, 2) according to the formulas listed in Table 2. This allowed us to obtain the relationship curve between $G(\alpha)$ and drying time t, as shown in Figure 2. Linear fitting of $G(\alpha)$ and drying time was performed using data analysis tools such as Origin, and the results are presented in Table 4.

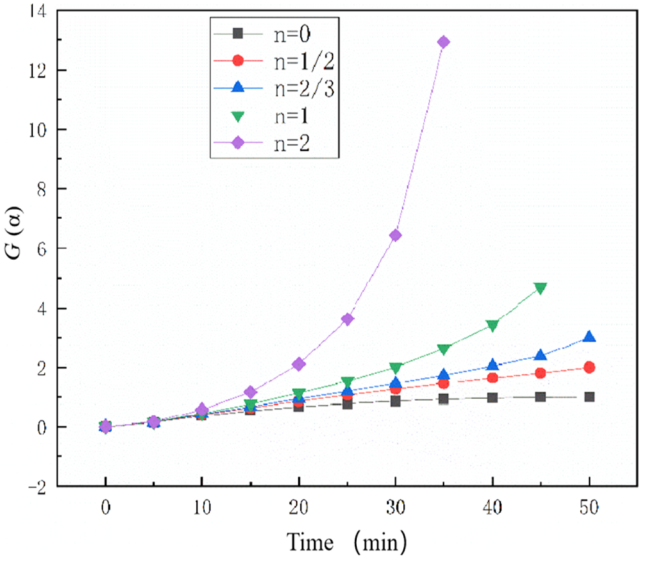

Figure 2. Relationship between raw iron slag $G(\alpha)$ and drying time.

Table 4. Straight-Line Fitting Results of the Mechanism Function of All Levels of Raw Iron Slag Drying

number of reaction progressions	fit a straight-line equation	R^2	squared residuals
0	$y = 0.15294 + 0.02029x$	0.89335	0.12028
1/2	$y = 0.01109 + 0.04068x$	0.99675	0.01336
2/3	$y = -0.15099 + 0.05708x$	0.98183	0.14893
1	$y = -0.50783 + 0.09709x$	0.92143	1.45974
2	$y = -2.12142 + 0.31408x$	0.71727	33.12982

Based on the fitting results in Table 4, it can be observed that the highest R^2 value is obtained when the reaction order is 1/2. This indicates that the linear fitting results for the drying of zinc smelting iron slag at 105 °C are best represented by a reaction order of 1/2. Therefore, it can be concluded that the drying kinetic model for the iron slag raw material follows a reaction order of 1/2.

3.2. Examination of the Arrhenius Equation for Ultrasonic Pretreatment of Iron Slag. The iron slag samples were pretreated under the following conditions: liquid-to-solid ratio of 4:1, ultrasonic frequency of 20 kHz, ultrasonic time of 20 s, and ultrasonic power of 70 W. After the pretreatment, the samples were subjected to drying at 105 °C. The resulting drying curve of the iron slag, along with the corresponding changes in solid content, is shown in Figure 3. The drying kinetics model was then calculated based on these experimental conditions.

The relationship between the solid content of ultrasonically pretreated iron slag and drying time was obtained from the experimental data in Figure 3. Using the formulas listed in Table 3, the integral form of the kinetic model function $G(\alpha)$ was calculated for different values of n (n = 0, 1/2, 2/3, 1, 2). This allowed for the derivation of the relationship curve between $G(\alpha)$ and drying time t, as shown in Figure 4. A linear fitting analysis was performed on $G(\alpha)$ and drying time t, and the results are presented in Table 5.

https://doi.org/10.1021/acsomega.3c07344
ACS Omega 2024, 9, 2578−2584

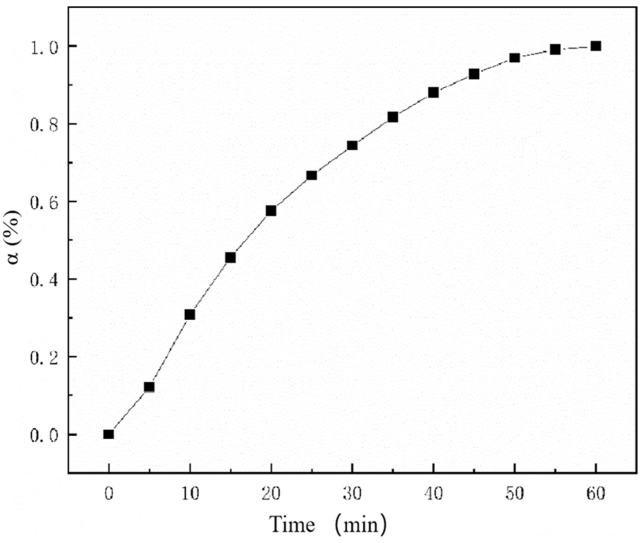

Figure 3. Characteristics of solid content variation in iron slag treated by ultrasonic.

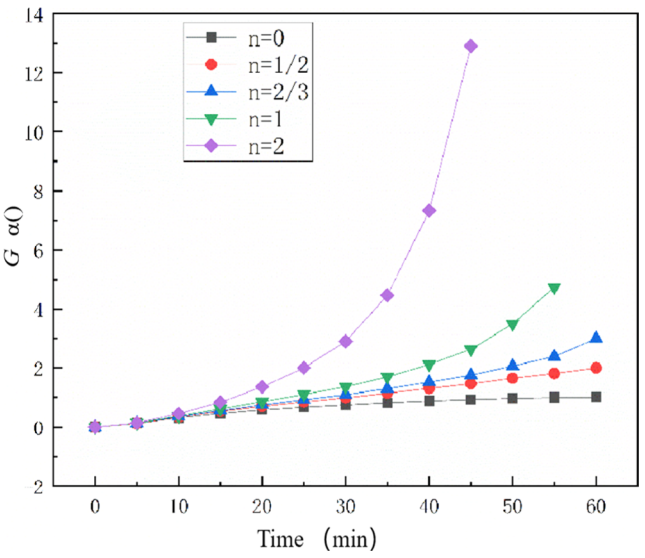

Figure 4. Relationship between $G(\alpha)$ and drying time of iron slag treated by ultrasonic.

Table 5. Straight-Line Fitting Results of the Mechanism Function at All Levels of Iron Slag Drying with Ultrasonic Pretreatment

number of reaction progressions	fit a straight-line equation	R^2	squared residuals
0	$Y = 0.1503 + 0.01667x$	0.91591	0.10563
1/2	$Y = 0.00171 + 0.033x$	0.99881	0.0054
2/3	$Y = -0.15875 + 0.04579x$	0.96761	0.29196
1	$Y = -0.49565 + 0.07589x$	0.89216	2.23805
2	$Y = -2.03725 + 0.2344x$	0.72176	37.23633

Based on the fitting results shown in Table 5, it can be observed that the maximum R^2 value is achieved when the reaction order is 1/2. This indicates that the linear fit obtained for the ultrasound pretreated iron slag at 105 °C drying conditions is the most optimal. Consequently, the reaction order of the drying kinetic model for ultrasound pretreated iron slag can be determined as 1/2.

3.3. Fitting of the Dynamic Model of the Empirical Formula for Iron Slag. The experimental data was analyzed and fitted using Origin software, and the results of the model fitting for the raw iron slag are presented in Table 6. The fitting curves for the raw iron slag are visualized in Figure 5.

Table 6. Fitting Results of Five Drying Kinetic Models of Raw Iron Slag

index number	model name	R^2	X^2	SSE
1	Henderson and Pbis	0.98077	0.0022	0.02417
2	Wang and Singh	0.99801	2.27569×10^{-4}	0.0025
3	Page	0.99677	3.68826×10^{-4}	0.00406
4	Lewis	0.97645	0.00269	0.03229
5	Wang	0.99647	4.03034×10^{-4}	0.00403

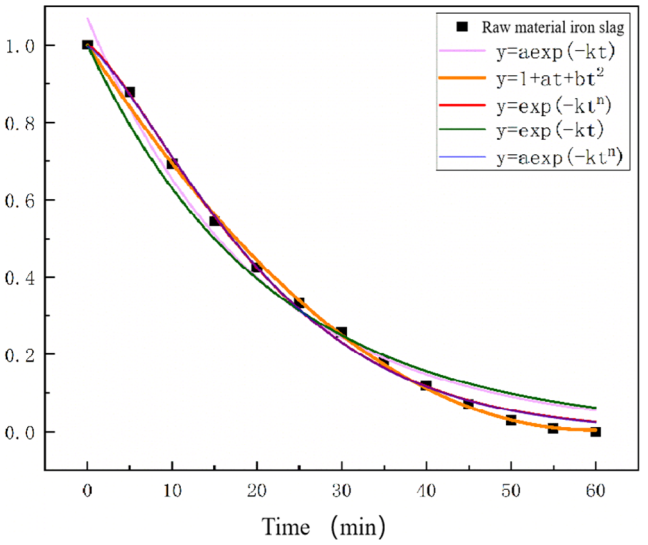

Figure 5. Fitting curve of raw material iron slag.

From Table 6, it can be observed that the model performance improves with higher correlation coefficients and smaller values of the chi-square and root-mean-square error. For the raw iron slag, all five models have a correlation coefficient greater than 0.97. Among them, the Wang and Singh model has the best fitting performance, with R^2 = 0.99801, $X^2 = 2.27569 \times 10^{-4}$, and SSE = 0.0025 being the optimal values among the five models. Additionally, from Figure 5, it can be seen that the predicted values of the function $y = 1 + at + bt^2$ are in better agreement with the actual measured values, indicating a better fitting performance. Therefore, the Wang and Singh model can be used to simulate the drying process of the raw iron slag.[30]

According to Table 7, for the raw iron slag under the optimal single-factor processing parameters, all five models have a correlation coefficient greater than 0.97. Among them, the Page model has the best fitting performance, with R^2 = 0.99898, $X^2 = 1.27547 \times 10^{-4}$, and SSE = 0.00115 being the optimal values among the five models. Additionally, the Page model has a simple equation form and fewer parameters. From the fitting curve of the ultrasound pretreated iron slag in Figure

https://doi.org/10.1021/acsomega.3c07344
ACS Omega 2024, 9, 2578−2584

Table 7. Fitting Results of Five Drying Kinetic Models of Ultrasonic Pretreatment Iron Slag

index number	model name	R^2	X^2	SSE
1	Henderson and Pbis	0.97522	0.00307	0.0276
2	Wang and Singh	0.99691	3.87459×10^{-4}	0.00349
3	Page	0.99898	1.27547×10^{-4}	0.00115
4	Lewis	0.97118	0.00361	0.0361
5	Wang	0.99886	1.4313×10^{-4}	0.00115

6, it can be seen that the function $y = \exp(-kt^n)$ is in better agreement with the actual measured values, indicating a better

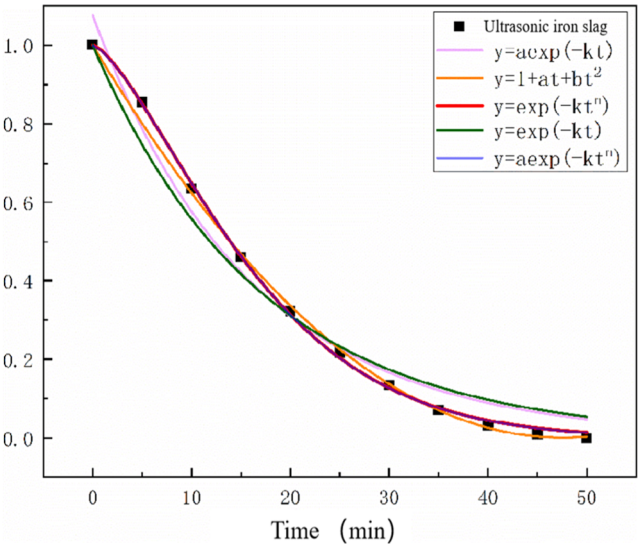

Figure 6. Fitting curve of ultrasonic pretreatment iron slag.

fitting performance. Therefore, the Page model can be used to simulate the drying process of the ultrasound pretreated iron slag.[31]

3.4. Energy Consumption Calculation. The formula for calculating the energy consumption is as follows

$$\text{energy consumption (kWh)} = \text{power (kW)} \times \text{time of use (h)} \quad (11)$$

From Figures 1 and 3, it is evident that ultrasonic pretreatment reduces the drying time of iron slag by approximately 10 min compared to untreated slag. The energy consumption required for the initial ultrasonic pretreatment is 3.89×10^{-4} kWh. At this stage, the amount of iron slag being processed is 15 g, and the oven's power is 500 W. The energy consumption during the 10 min drying process is 8.30×10^{-2} kWh. With ultrasonic pretreatment, each 15 g of iron slag's drying process can save approximately 8.26×10^{-2} kWh. Scaling up this model, drying one ton of iron slag can save approximately 550 kWh, highlighting its crucial role in energy conservation and its immense development potential.

4. CONCLUSIONS

The Arrhenius equation reveals that the reaction order of zinc smelting iron slag remains constant at 1/2, both before and after ultrasonic treatment. This indicates that the reaction rate is directly proportional to the square root of the reactant concentration. Despite an increase in the drying rate of the iron slag under the influence of ultrasonic pretreatment, the characteristic of a 1/2 order reaction is retained.

Empirical formula kinetic model fitting reveals a shift in the applicable kinetic model for zinc smelting iron slag before and after ultrasonic treatment. The drying kinetics of untreated iron slag aligns with the Wang and Singh model, while the drying kinetics of ultrasonically pretreated iron slag fits the Page model.

The primary function of the Page model is to fit experimental data, determining the drying rate constant k and the Page index "n". This allows for the prediction of the drying rate and drying time of ultrasonically pretreated iron slag. The model serves as a tool for optimizing the drying process and enhancing efficiency, and it can be employed to compare the drying performance under varying conditions.

The use of ultrasonic pretreatment for drying iron slag can save energy and has immense potential for promoting green and sustainable development.

AUTHOR INFORMATION

Corresponding Author

Linqing Dai − *National Local Joint Laboratory of Engineering Application of Microwave Energy and Equipment Technology, Kunming, Yunnan 650093, China; Faculty of Metallurgical and Energy Engineering, Kunming University of Science and Technology, Kunming, Yunnan 650093, China;* orcid.org/0000-0003-0672-1477; Email: linqingdai@163.com

Authors

Yue Cheng − *National Local Joint Laboratory of Engineering Application of Microwave Energy and Equipment Technology, Kunming, Yunnan 650093, China; Faculty of Metallurgical and Energy Engineering, Kunming University of Science and Technology, Kunming, Yunnan 650093, China;* orcid.org/0009-0005-2994-6216

Libo Zhang − *National Local Joint Laboratory of Engineering Application of Microwave Energy and Equipment Technology, Kunming, Yunnan 650093, China; Faculty of Metallurgical and Energy Engineering, Kunming University of Science and Technology, Kunming, Yunnan 650093, China;* orcid.org/0000-0003-3244-0142

Bo Yu − *National Local Joint Laboratory of Engineering Application of Microwave Energy and Equipment Technology, Kunming, Yunnan 650093, China; Faculty of Metallurgical and Energy Engineering, Kunming University of Science and Technology, Kunming, Yunnan 650093, China*

Chuxuan Yang − *National Local Joint Laboratory of Engineering Application of Microwave Energy and Equipment Technology, Kunming, Yunnan 650093, China; Faculty of Metallurgical and Energy Engineering, Kunming University of Science and Technology, Kunming, Yunnan 650093, China*

Liang Zhou − *National Local Joint Laboratory of Engineering Application of Microwave Energy and Equipment Technology, Kunming, Yunnan 650093, China; Faculty of Metallurgical and Energy Engineering, Kunming University of Science and Technology, Kunming, Yunnan 650093, China*

Baichuan Lou − *Nanjing Greentown Real Estate Co Ltd., Nanjing, Jiangsu 210000, China*

Complete contact information is available at: https://pubs.acs.org/10.1021/acsomega.3c07344

https://doi.org/10.1021/acsomega.3c07344
ACS Omega 2024, 9, 2578−2584

Author Contributions

L.D.: investigation, formal analysis, and conceptualization. Y.C.: writing—review and editing. L.Z.: conceptualization, supervision, and validation. B.Y.: conceptualization. C.Y.: conceptualization. L.Z.: conceptualization. B.L.: conceptualization.

Notes

The authors declare no competing financial interest.

■ ACKNOWLEDGMENTS

The authors extend their appreciation to the Researchers Supporting Project number (202107AA110002), Kunming University of Science and Technology for supporting this research. In addition, the authors would like to thank the National Local Joint Laboratory of Engineering Application of Microwave Energy and Equipment Technology.

■ REFERENCES

(1) Wang, X. B.; Li, X. Y.; Yan, X.; Tu, C.; Yu, Z. G. Environmental risks for application of iron and steel slags in soils in China: A review. *Pedosphere* **2021**, *31* (1), 28−42.

(2) Katarzyna, M.; Grzegorz, I.; Dawid, S.; Katarzyna, C.; et al. Value-added strategies for the sustainable handling, disposal, or value-added use of copper smelter and refinery wastes. *J. Hazard. Mater.* **2021**, *403*, No. 123602.

(3) de Araújo Neto, A. P.; Sales, F. A.; Ramos, W. B.; Brito, R. P. Thermo-environmental evaluation of a modified Waelz process for hazardous waste treatment. *Process Saf. Environ. Prot.* **2021**, *149*, 442−450.

(4) Rongzhen, C.; Xialu, L.; Qingchun, G. A novel multinuclear zinc complex Zn-Bet-Tf 2 N for electroplating wastewater treatment using forward osmosis technique. *Chem. Eng. J.* **2021**, *404*, No. 126569.

(5) Tahir, H. S.; Saqib, S. T.; Ayaz, A. S.; Lasse, A. R. Catalytic hydrothermal liquefaction of contaminated construction wood waste for biocrude production and investigation of fate of heavy metals. *Fuel Process. Technol.* **2021**, *212*, No. 106621.

(6) Zhu, H.; Shang, Y.; Du, J.; Zhou, C.; Liu, X. A Fuzzy Control Method Based on Rule Extraction for Zinc Leaching Process of Zinc Hydrometallurgy. *Min. Metall. Explor.* **2023**, *40* (4), 1321−1331.

(7) Feiyun, T.; Jiayuan, W.; Jiquan, Fu.; Yi, Y. Titanium and zinc-containing nanoparticles in estuarine sediments: Occurrence and their environmental implications. *Sci. Total Environ.* **2021**, *754*, No. 142388.

(8) Zhong, M. B. T.; Gururaj, P.; Vyasaraj, M.; Anoj, G. Using low-temperature sinterless powder method to develop exceptionally high amount of zinc containing Mg−Zn−Ca alloy and Mg−Zn−Ca/SiO_2 nanocomposite. *J. Alloys Compd.* **2021**, *853*, No. 156957, DOI: 10.1016/j.jallcom.2020.156957.

(9) Mancini, A.; Lothenbach, B.; Geng, G.; Grolimund, D.; Sanchez, D. F.; Fakra, S. C.; Wieland, E.; et al. Iron speciation in blast furnace slag cements. *Cem. Concr. Res.* **2021**, *140*, No. 106287.

(10) Waldmüller, W.; Herdzik, S.; Gaderer, M. Combined filtration and oxalic acid leaching for recovering phosphorus from hydrothermally carbonized sewage sludge. *J. Environ. Chem. Eng.* **2021**, *9* (1), No. 104800.

(11) Patrick, M.; Adrian, A.; Henning, S.; Hermann, N. In-situ cleaning process of chamber filter presses with sensor-controlled and demand-oriented automation. *Sep. Purif. Technol.* **2021**, *256*, No. 117793.

(12) Xirui, W.; Gad, L.; Stuart, L. Green and scalable separation and purification of carbon materials in molten salt by efficient high-temperature press filtration. *Sep. Purif. Technol.* **2021**, *255*, No. 117719.

(13) Safonov, D.; Kinnarinen, T.; Häkkinen, A. An assessment of Blaine's air permeability method to predict the filtration properties of iron ore concentrates. *Miner. Eng.* **2021**, *160*, No. 106690.

(14) Guo, Z.; Deqing, Z.; Jian, P.; Xincheng, Y.; et al. Efficient and green treatment of ultrapure magnetite to prepare powder metallurgy iron powders. *Powder Technol.* **2021**, *378*, 19−28.

(15) Moser, K.; Wopienka, E.; Pfeifer, C.; Schwarz, M.; Sedlmayer, I.; Haslinger, W. Screw reactors and rotary kilns in biochar production − A comparative review. *J. Anal. Appl. Pyrolysis* **2023**, *174*, No. 106112, DOI: 10.1016/J.JAAP.2023.106112.

(16) Lian, L.; Zong, X.; He, K.; Yang, Z. Soft sensing of calcination zone temperature of lime rotary kiln based on principal component analysis and stochastic configuration networks. *Chemom. Intell. Lab. Syst.* **2023**, *240*, No. 104923, DOI: 10.1016/J.CHEMOLAB.2023.104923.

(17) Kern, S.; Michael, H.; Gerhard, K.; Hermann, H.; et al. Rotary kiln pyrolysis of straw and fermentation residues in a 3MW pilot plant − Influence of pyrolysis temperature on pyrolysis product performance. *J. Anal. Appl. Pyrolysis* **2012**, *97*, 1−10.

(18) Yi, L.; Zhang, N.; Liang, Z.; Wang, L.; Xiao, H.; Huang, Z. Coal ash induced ring formation in a pilot scale rotary kiln for low-grade iron ore direct reduction process: Characterization and mechanism. *Fuel* **2022**, *310*, No. 122342, DOI: 10.1016/j.fuel.2021.122342.

(19) Ge, L.; Feng, Y.; Dai, Y.; Wang, R.; Ge, T. Imidazolium-based ionic liquid confined into ordered mesoporous MCM-41 for efficient dehumidification. *Chem. Eng. J.* **2023**, *452* (P1), No. 139116, DOI: 10.1016/j.cej.2022.139116.

(20) Guo, Z.; Liping, M.; Quxiu, D.; Lichun, W.; et al. Dewatering performance of sewage sludge under pretreatment with modified corn-core powder. *Sci. Total Environ.* **2019**, *684*, 402−412.

(21) Zhang, J.; Luo, C. P.; Yang, L. Nickel/Cobalt-Catalyzed Reductive Hydrocyanation of Alkynes with Formamide as the Cyano Source, Dehydrant, Reductant, and Solvent. *Adv. Synth. Catal.* **2021**, *363* (1), 283−288.

(22) Liu, Y. X.; Liang, Q. F.; Liu, Y.; Rashid, A.; Qayum, A.; Ma, H.; Ren, X. F. Effects of multi-frequency ultrasound on sodium caseinate/pectin complex: Emulsifying properties, interaction force, structure and correlation. *Int. J. Biol. Macromol.* **2023**, *242* (P2), No. 124801, DOI: 10.1016/j.ijbiomac.2023.124801.

(23) Gómez-Salazar, J. A.; Galván, N. A.; Lorenzo, J. M.; Sosa, M. M. E. Ultrasound effect on salt reduction in meat products: a review. *Curr. Opin. Food Sci.* **2021**, *38*, 71−78.

(24) Azam, A.; Asghar, R.; Seyed, M. H. M.; Seyed, M. H. H. Ultrasonic potential in maintaining the quality and reducing the microbial load of minimally processed pomegranate. *Ultrason. Sonochem.* **2021**, *70*, No. 105302.

(25) Ambedkar, B. *Ultrasonic Coal-Wash for De-Ashing and De-Sulfurization*, Springer: Berlin, Heidelberg, 2012.

(26) Chen, L.; Xu, Q.; Boettcher, S. W. Kinetics and mechanism of heterogeneous voltage-driven water-dissociation catalysis. *Joule* **2023**, *7* (8), 1867−1886.

(27) Zhang, Y.; Chen, S.; Ruan, S.; Wang, W.; Wang, Q.; Chen, D.; Liu, Y.; Yan, D. Electrothermal effect of alternating current on hardening process of metakaolin-based geopolymer. *Cem. Concr. Compos.* **2023**, *142*, No. 105205, DOI: 10.1016/J.CEMCONCOMP.2023.105205.

(28) Huang, M.; Jiang, J.; Wang, Y.; Liu, Y.; Zhang, Y.; Dong, J. Comparison and error evaluation of Arrhenius model and typical machine learning algorithms for high-temperature flow stress prediction of GH3536 superalloy. *Mater. Lett.* **2023**, *349*, No. 134754, DOI: 10.1016/J.MATLET.2023.134754.

(29) Huimin, Y. In *Ultrasonic Sensor and In-Situ Correction for the Monitoring of Indistinct Interface Level*, International Conference on Sensors and Control Techniques (ICSC 2000). Vol. 4077. SPIE, 2000; pp 145−148.

(30) Zongliang, Z.; Siyi, L.; Sihong, L.; Xuejun, B. Thermokinetics of mass-loss behavior on direct reduction of copper slag by waste plastic char. *Chem. Eng. J.* **2021**, *406*, No. 126671, DOI: 10.1016/j.cej.2020.126671.

(31) Xin, X.; Lei, Z.; Yabin, F.; Yanhui, S. Ultrasound freeze-thawing style pretreatment to improve the efficiency of the vacuum freeze-drying of okra (Abelmoschus esculentus (L.) Moench) and the

https://doi.org/10.1021/acsomega.3c07344
ACS Omega 2024, 9, 2578−2584

quality characteristics of the dried product. *Ultrason. Sonochem.* **2021**, *70*, No. 105300.

https://doi.org/10.1021/acsomega.3c07344
ACS Omega 2024, 9, 2578−2584